Colloids and Surfaces B: Biointerfaces 188 (2020) 110753

Contents lists available at ScienceDirect

Colloids and Surfaces B: Biointerfaces

journal homepage: www.elsevier.com/locate/colsurfb

Polyphotosensitizer nanogels for GSH-responsive histone deacetylase inhibitors delivery and enhanced cancer photodynamic therapy

Nian Liu[a], Hongsen Liu[c], Haoran Chen[b], Gang Wang[a], Haolin Teng[a], Yulei Chang[b,*]

[a] Department of Urology, The First Hospital, Jilin University, Changchun, Jilin, 130021, China
[b] State Key Laboratory of Luminescence and Applications, Changchun Institute of Optics, Fine Mechanics and Physics, Chinese Academy of Sciences, Changchun, 130033 Jilin, China
[c] School of Life Sciences, Jilin University, Changchun,130012, China

ARTICLE INFO

Keywords:
HDACi
Photodynamic therapy
Nanogel
Polyphotosensitizer
Imaging

ABSTRACT

Photodynamic therapy (PDT) is one of the non-invasive and selective treatment methodologies for cancer. However, many highly efficient photosensitizers (PSs) are usually low physiological solubility, limited bioavailability and tending aggregation, impeding the effectiveness of PDT, as well as cancer resistance of PDT further reduce its therapeutic effect. Though some smart delivery systems have been developed, the problem of photosensitizer leakage/release has not been completely solved. Herein, we developed a smart therapeutic nanoplatform based on polyphotosensitizer nanogel as novel nanophotosensitizers and drug carriers. Moreover, by loading of histone deacetylase inhibitors (SAHA), it allows for enhanced synergistic therapy strategy of prostate cancer via inhibiting HIF-1α and VEGF pathways of cancer cells involved in PDT resistance. Our study presents the well-designed nanoplatform of nanogel-Ce6, which could serve as a photodynamic agent without Ce6 molecules release in the responsive environment, offering the potential to encapsulate diverse functional components for smart drug release and imaging-guided combination therapy *in vitro and in vivo*.

1. Introduction

Photodynamic therapy (PDT) is a promising non-invasive and selective activation of the therapeutic modality in cancers [1–3], which relies on the photosensitizers to absorb the excitation energy of appropriate wavelength to relax to the excited triplet state and then transfer to the surrounding oxygen to generate singlet oxygen (Type II) [4,5], or transfer an electron to generate other reactive oxygen species (ROS, Type I) [1,6,7]. This modality of therapy can selectively damage the cancer cells and induce cell death by cytotoxic species without induction of resistance [8,9]. Efforts have been made to improve the efficacy of PDT and biosafety by developing a new generation of photosensitizer (PS) [10,11]. However, it remains a challenge to perform PDT for cancer in clinical applications due to most of the photosensitizers are low water-soluble and uncontrollable bio-distribution resulting in quick body clearance, limited tumor-selective delivery and even lowering the ROS yields (owing to they are prone to aggregates in aqueous media).

To address limitations above, encapsulating the PSs into the carriers provides a promising strategy towards improved control of PS distribution and tumor-selective delivery [12]. However, the leakage/release of the PSs will also generate the aggregates, resulting in a decrease of fluoresces and singlet oxygen yield (self-quenchability) [13]. Therefore, the conjugating/cross-linking of the PSs in the carrier's network should be a better strategy. Among the various PSs, a second-generation photosensitizer— chlorin e6 (Ce6) is an attractive one with deep red fluorescence emission and high singlet oxygen yield [14], which has been applied to many types of tumor treatment [15]. To optimize pharmacokinetics, some smart nanosized drug delivery systems have been extensively investigated for precise drug release, including Ce6 photosensitizer [16–18]. For example, Hou et al., have reported that conjugated ce6 with a redox-responsive cleavable disulfide linker to achieve better efficacy and less off-target side effects in cancer treatment. However, the redox environment will lead to Ce6 release [18,19], causing the re-aggregation of Ce6. Therefore, the effect of PDT can only be improved in a limited way. Considering the polymerization of Ce6 in the networks of carriers via double bonds polymerization of Ce6, the nanogel would be one of the best candidates.

Nanogel is nanoscopic of a hydrogel, which are cross-linked polymer networks capable of absorbing large quantities of biological fluids [20–22]. For PDT applications, a considerable number of hydrogel-based PSs biomaterials have been designed [23] via

* Corresponding author.
E-mail address: yuleichang@ciomp.ac.cn (Y. Chang).

https://doi.org/10.1016/j.colsurfb.2019.110753
Received 4 October 2019; Received in revised form 10 December 2019; Accepted 20 December 2019
Available online 23 December 2019

encapsulation, conjugation or copolymerization [13,24]. As hydrogel, the nanosized one (nanogel) offers the potential for long blood circulation and preferential delivering to the desired site of action, such as the tumor tissues [16]. Therefore, the development of Ce6-based nanogel not only as a nanophotosensitizer but also as a carrier is favorable in PDT and on-demand drug delivery of tumor. It allows for high efficiency of PDT synergistic other therapy modalities to improve the curative effect of cancer. Considering the tumor microenvironment is altered after PDT treatment which has effects on survival of tumor cells [25]. Moreover, a hypoxic condition in the surviving tumor cells can cause the stabilization of hypoxia-inducible factor 1α (HIF-1α) and increase the expression of VEGF by HIF-1α pathway, which promotes the tumor angiogenesis and enhances tumor proliferation [26–28]. Given by these, to decrease the level of HIF-1α and VEGF, suberoylanilide hydroxamic acid (SAHA), one of the FDA approved histone deacetylase (HDAC) inhibitors can solve the problems above, which has shown potent inhibitory effects on the hypoxia signaling pathway in some studies [29,30].

Herein, we demonstrated a versatile one-pot approach for the direct synthesis of polyphotosentizer nanogels as nanophotosensitizer for PDT and drug carrier application in a combination of PDT and HDAC inhibition for enhanced synergistic therapy strategy of prostate cancer (Scheme 1). In our design, the glutathione sensitive nanoplatform containing varying amounts of Ce6 itself as the monomer was obtained. Importantly, the stimuli-responsive triggered drug release of SAHA will not induce the release of Ce6, ensuring the high efficiency of PDT. The encapsulated SAHA allowed for improving the antitumor activities via inhibiting HIF-1α and VEGF pathways of cancer cells involved in PDT resistance, as well as reducing severe side effects of SAHA in current clinical treatments.

2. Materials and methods

2.1. Materials

N-isopropyl acrylamide (NIPAM) N, N'-bis (acryloyl) cystamine (BAC) were purchased from J&K. KPS and 2-acrylamide-2-methyl propane sulfonic acid (AMPS) were purchased from Aladdin. DAPI and DPBF and DCFH-DA were obtained from Beyotime. Chlorin e6 (Ce6, 90 %) was purchased from Yuanye, Shanghai. Vorinostat (SAHA) was obtained from Selleck. CCK8 kit (Multisciences Biotech. Hangzhou).

2.2. The synthesis of dual-sensitive nanogel-Ce6

The nanogel-Ce6 was synthesized by emulsion polymerization according to our reported method with some modification [31]. Typically, the calculated amount of NIPAM, AMPS, and cross-linker BAC were added sequentially to the flask and dissolved in 8 mL DI-water. Afterward, the surfactant of SDS (0.04 wt %) was added. The mixture was stirred at 400 rpm under an argon gas atmosphere to remove the dissolved oxygen. After that, it was heated up to 70 °C and kept for 1 h. Then, 15 mL of the initiator (KPS, 10 mg/mL) was added to initiate the polymerization and the monomer Ce6 was added subsequently. The polymerization was kept at 70 °C for 5 h. The resulting nanogel were purified by dialysis for 7 days and then lyophilized to obtain the nanogel-Ce6 for further use. The Ce6 free nanogel was also prepared for the encapsulation of Ce6 molecules as the control group.

2.3. Drug loading and release profile

To encapsulate the SAHA into the nanogel-Ce6 networks, a film hydration method was employed. Briefly, nanogel and SAHA were dissolved in methanol (2 mL) and then the dried nanogel film was obtained by evaporation of methanol. After adding DI-water (2 mL) to the nanogel-Ce6/SAHA film, the formed nanoplatform (nanogel-Ce6-SAHA) in the aqueous media were size-homogenized by sonication for 5 min and then additionally by filtration to remove their large size distribution. The drug loading efficiency was calculated by UV–vis and HPLC. Similarly, the Ce6 encapsulated in the free nanogel group was also obtained (labeled as nanogel/Ce6).

The cumulative release of SAHA was studied by a dialysis method. Briefly, the nanogel-Ce6-SAHA solution was transferred to the dialysis bag and immersed in PBS buffer at 37 °C with gentle shaking. After that, fresh PBS buffer solution replaced the external fluid membrane at the determined time points. For GSH-mediated SAHA release, a similar method was adopted in addition to different GSH concentration treatment. The concentrations of SAHA were monitored and recorded by the HPLC-UV. The Ce6 release profiles from nanogel-Ce6 and nanogel/Ce6 were studied respectively. The absorbance of the solution is measured and recorded around 660 nm by the UV–vis spectrophotometer, and the concentration of Ce6 was determined based on a calibration curve. The standard working curves of Ce6 and SAHA were provided as Fig. S1 (ESI), respectively.

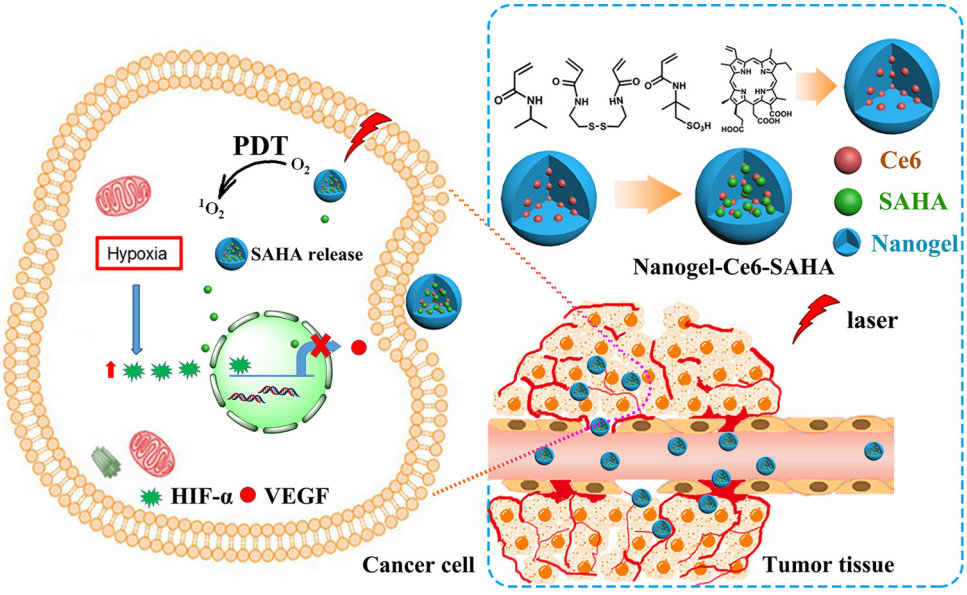

Scheme 1. One-pot synthesis of nanogel-Ce6 and the combination of PDT and HDACi for enhanced PCa synergistic therapy.

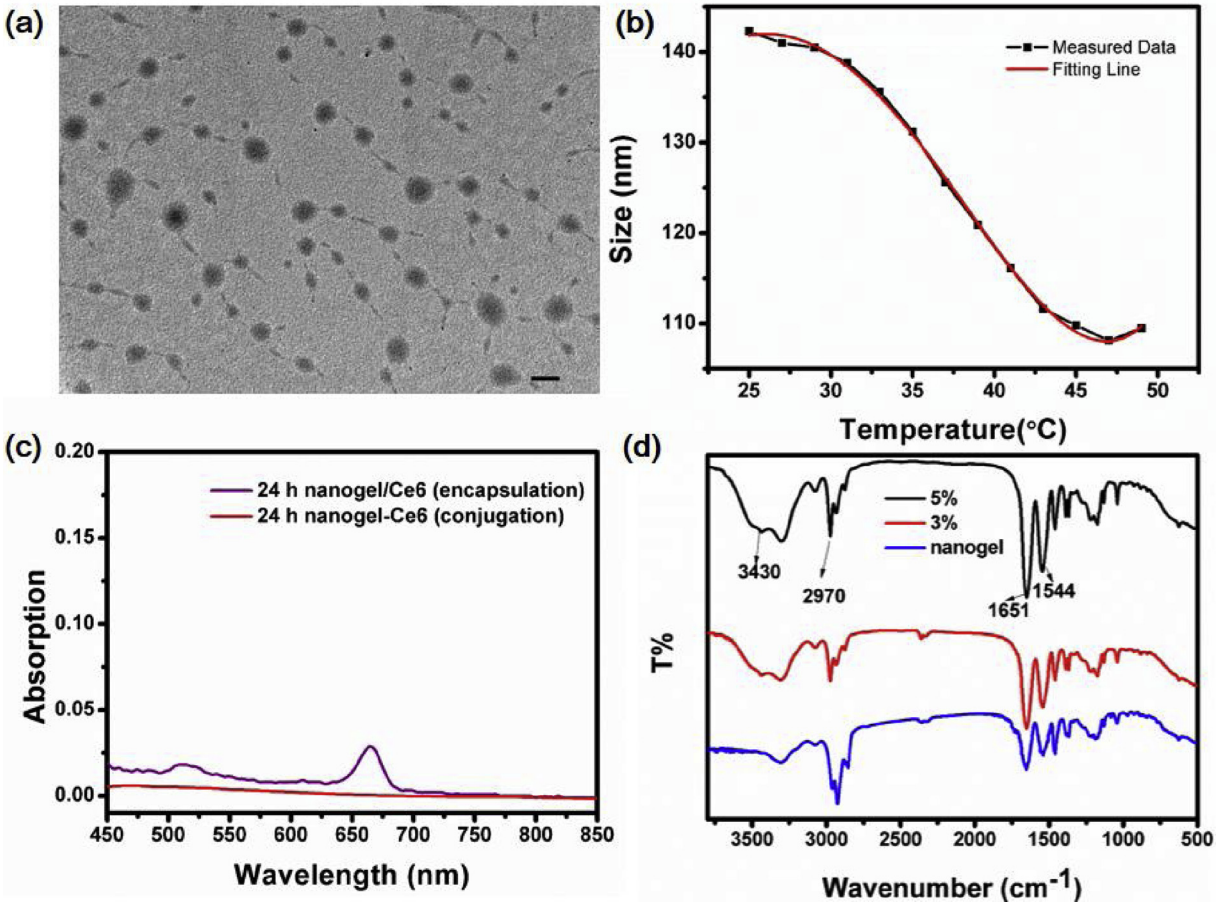

Fig. 1. (a) TEM image of nanogel-Ce6 (3 %), scale bar = 100nm, (b) VPTT of nanogel-Ce6 (3 %), (c) The leakage of photosensitizer Ce6 from nanogel-Ce6 and nanogel/Ce6, and (d) the FT-IR spectra of nanogel, nanogel-Ce6 (3 %) and nanogel-Ce6 (5 %).

2.4. Singlet oxygen detection

The DPBF probe was employed to detect the generation of singlet oxygen. Typically, a certain of nanogel-Ce6 was mixed with DPBF (10 μL, 2 mg/mL in ethanol). The mixture was transferred to a 1 cm × 1 cm cell and irradiated with a 655 nm laser at 25 mW/cm^2 at determined time points. The DPBF consumption was recorded by a miniature spectrometer (USB4000-UV-VIS).

2.5. Cellular uptake and in vitro cytotoxicity

2.5.1. Cellular uptake and proliferation assay

Human prostate cancer cell line PC-3 cells (The American Type Culture Collection) and mouse prostate cancer cell line RM-1 (Cell Bank of Type Culture Collection, Shanghai) were cultured in RPMI 1640supplemented with 10 % fetal bovine serum, 100 U/mL penicillin, and 100 μg/mL streptomycin at 37 °C with 5 % CO_2. Ce6, nanogel-Ce6 were dissolved in PBS. SAHA was dissolved in DMSO. For investigation of intracellular uptake and distribution of nanogel-Ce6, cells were incubated with 10 mg/mL nanogel-Ce6 for different times (3 h, 6 h) at 37 °C and washed with PBS three times, then fixed by 4 % paraformaldehyde for 15 min, and stained by DAPI (0.1 mg/mL) for 10 min in the dark. The cells were washed by PBS three times, then observed with a Nikon confocal microscope. The cells were treated with Ce6 (3 h and 6 h) as the control.

Cell Counting Kit 8 cell proliferation assay was used to evaluate cell proliferation according to the manufacturer's instructions. PC-3 cells were seeded in 96-well plates at a density of 5 × 10^4/well and incubated at 37 °C for 24 h. Ce6 (3 μg/mL), nanogel-Ce6(10 mg/mL), nanogel-Ce6-SAHA (10 mg/mL), SAHA (5 μM) were added to the wells respectively 4 h prior to exposure to the 655 nm light at 50 mW/cm^2 for 10 s and 20 s. Cells were cultured for another 24 h, then 10 μL of CCK-8 reagent was added to each well then incubated at 37 °C for 1.5 h, the absorbance was determined at 450 nm with the microplate reader.

2.5.2. Cell apoptosis analysis

Annexin-V-fluorescein isothiocyanate (FITC) and propidium iodide (PI) staining were performed using an Annexin-V-FITC/PI kit (BD) according to the manufacturer's instructions. Briefly, PC-3 cells were cultured in 6-well plates and treated with different reagents for 4 h, then the cells were exposed to the light. Cells were harvested using 0.05 % trypsin after 24 h incubation and washed twice with cold PBS, and then suspended in binding buffer. 1 × 10^5 cells with 100 μL binding buffer were added to a tube and incubated with 5 μL of Annexin-V-FITC and 5 μL of PI. Cells were gently mixed and incubated for 15 min at room temperature. 400 μL binding buffer was then added to each tube. The samples were analyzed by Flow cytometer (BD Biosciences). Experiments were repeated three times.

2.6. Imaging and antitumor efficacy

2.6.1. Tumor model and treatments

All the animal procedures were performed following a protocol approved by the Jilin University Animal Care and Use Committee. For tumor models, male C57BL/6 mice aged 7 weeks (Changsheng biotechnology, Liaoning) were inoculated subcutaneously with 4 × 10^5 RM-1 cells in 0.1 mL PBS. After 1 week, mice with palpable tumors were selected for the therapeutic study. The imaging-guided strategy

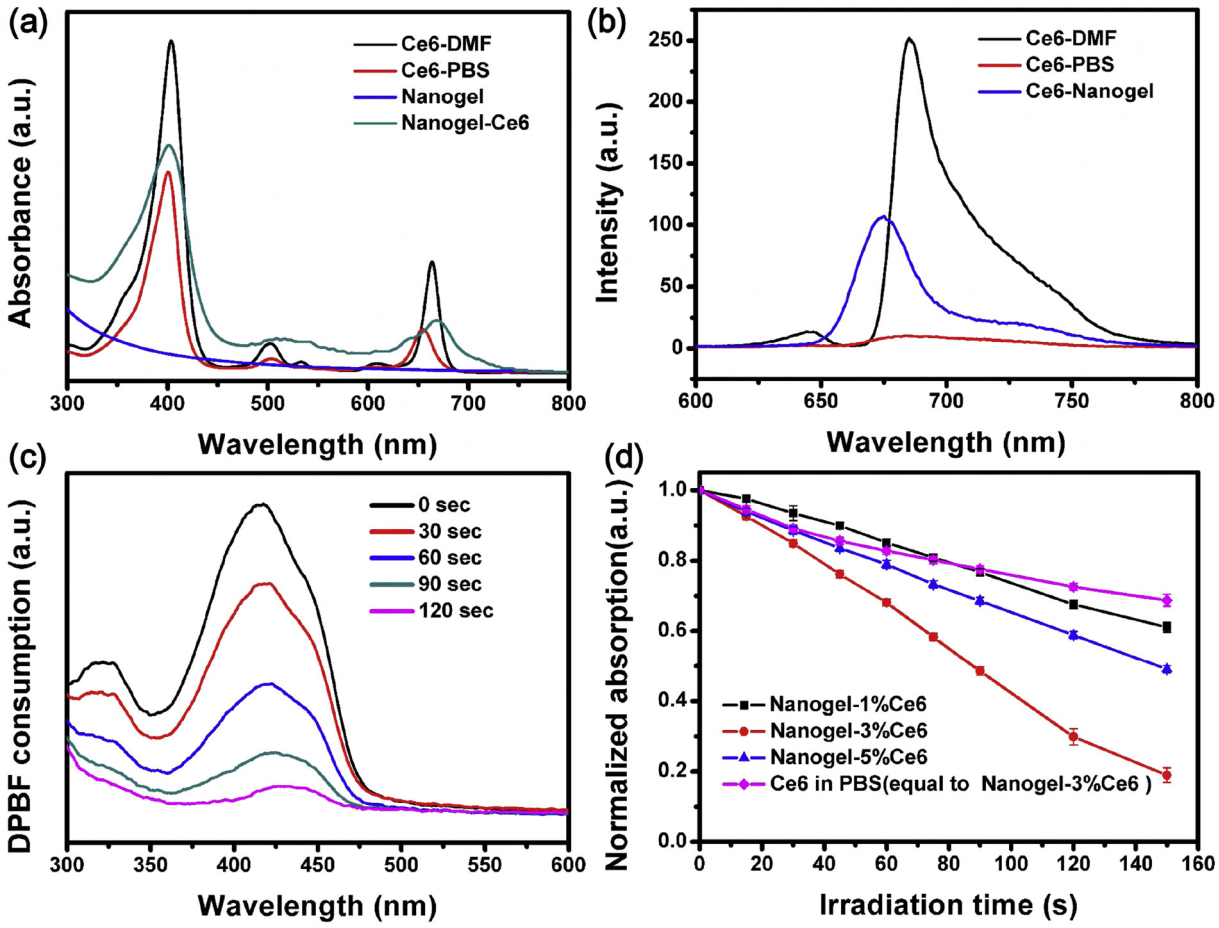

Fig. 2. (a) UV–vis absorption spectra of Ce6 in DMF and PBS, and nanogel with/without Ce6 in H_2O; (b) Fluorescence emission spectra of Ce6 in DMF, PBS and nanogel-Ce6; (c) Consumption of DPBF overtime under 655nm light irradiation, and (d) Consumption of DPBF overtime for different weight percentage of polymerized Ce6 with the same power density of 655nm laser light.

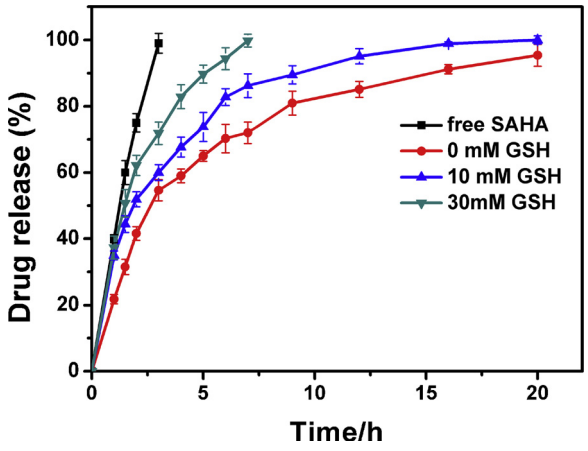

Fig. 3. (a) Free SAHA release and (b) SAHA release from nanoplatform. GSH stimulus SAHA release from nanoplatform with (c) 10 mM and (d) 30mM, respectively. Data are represented as means ± SDs.

was adapted to visualize the tumor and monitor drug distribution, as well as acquire the treatment timing. For the imaging study, the normal mice and tumor-bearing mice were *i.v.* injected with nanogel-Ce6-SAHA (100 μL, 33 mg/mL), respectively and measured at determined time points. After that, for PDT groups, each of them received Ce6, nanogel-Ce6, nanogel-Ce6-SAHA, and SAHA via *i.v.* injection. The mice were illuminated with an irradiance of 50 mW/cm^2 light at 655 nm for 240 s after 12 h post-injection. Tumor size and body weight were measured every 2 days after treatment.

2.6.2. Histological and immunohistochemical studies

For H&E staining and immunohistochemical procedures, one part of the tumor tissue was fixed in formalin. Paraffin-embedded 2 μm thick tumor sections were analyzed by immunohistochemical analysis for VEGF and HIF-1α. Sections were deparaffinized, rehydrated in PBS, and microwaved for 10 min for antigen retrieval. Endogenous peroxidase activity was quenched with 3 % hydrogen peroxide for 15 min, then blocked with 10 % normal goat serum for 15 min. The sections were incubated overnight at 4 ℃ with VEGF Ab (diluted 1:50, Bioss, China) and HIF-1α Ab (diluted 1:50, Novus, CO, USA). Samples were incubated with goat anti-mouse and goat anti-rabbit secondary antibody.

2.7. Statistical analysis

Statistical analysis was conducted by making use of analysis of variance (Student's t-test). All data were presented as mean ± standard deviation. P-value < 0.05 was considered statistically significant.

3. Results and discussion

3.1. preparation and characterization of nanogel-Ce6

Poly (NIPAM-co-AMPS-Ce6) nanogels as PDT carriers were synthesized in one pot, in which Ce6 molecules as functional monomers were polymerized in the backbone and BAC as a cross-linker was employed

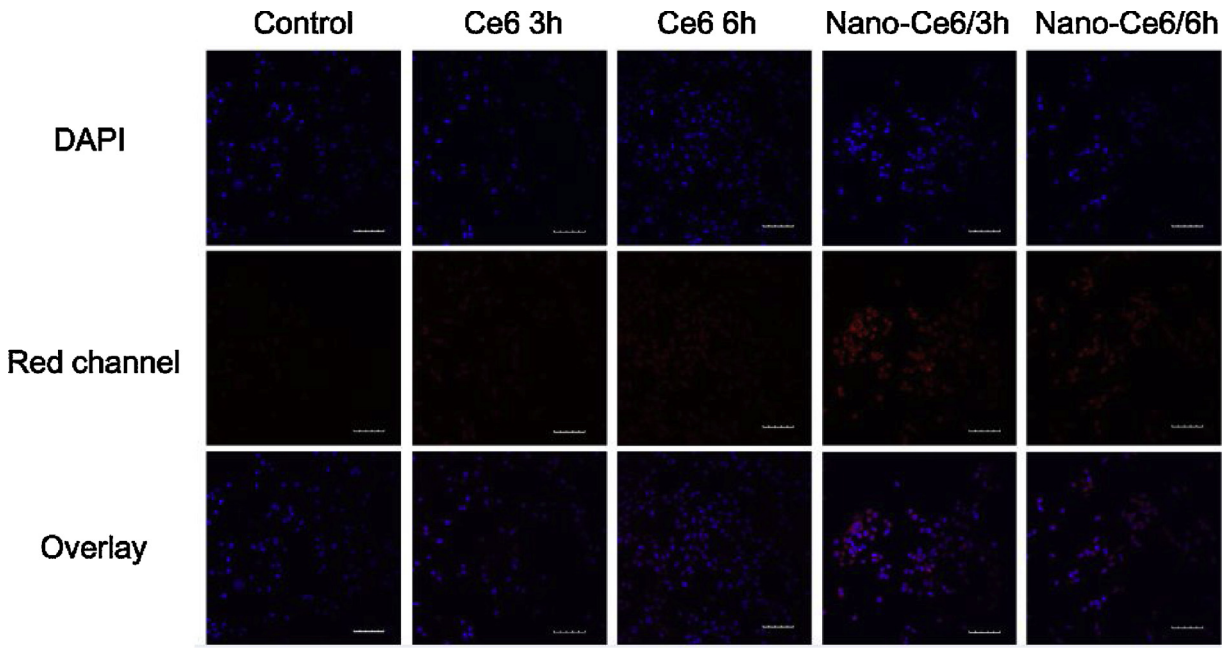

Fig. 4. Cell uptake of Ce6 and nanogel-Ce6 at different times (3h and 6h). Scale bars are 50μm.

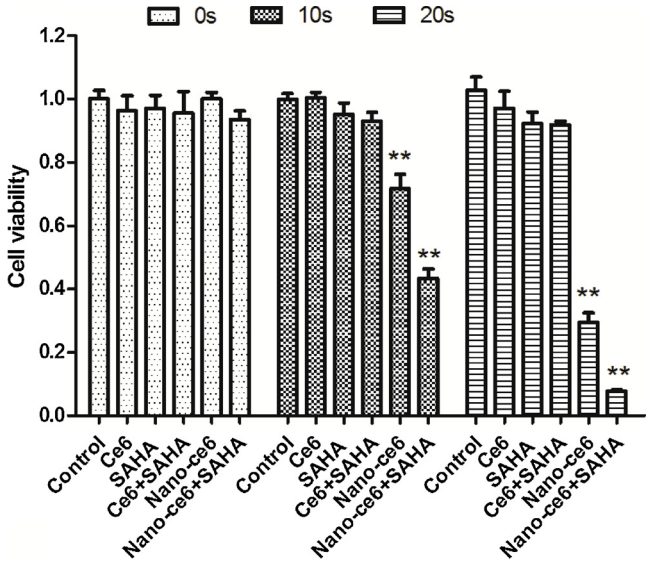

Fig. 5. Cell viability of PC-3 cells with different treatments under light irradiation (655nm, 50mW/cm^2 for 0s, 10s, and 20s). Data are shown as the mean ± SD (n = 3). $P < 0.05$.

for redox-responsive drug delivery. To enhance the antitumor activities of PCa, an HDACi drug of SAHA was encapsulated in this nanoplatform. The morphology and size of nanogels are illustrated in Fig. 1.

The morphology and size of nanogel-Ce6 (3 %, w/w, optimal concentration) were measured by TEM as shown in Fig. 1a. We can see that the nanogel-Ce6 was near-spherical with a mean diameter of 68.6 nm. The properties of the different amounts of polymerized Ce6 in nanogel-Ce6 NPs were also studied by DLS. DLS analysis at 25 ℃ for the nanogel-Ce6 with different concentrations of Ce6 (1 %, 3 %, and 5 %, w/w), indicated a mean diameter of 114.8 ± 1.27, 138.6 ± 0.27, and 140.1 ± 0.78 nm, and the PDI of 0.115, 0.015, and 0.092, respectively. Furthermore, it is known that PNIPAM system exhibit a demixing phase transition with a lower critical solution temperature (LCST) around 32 ℃, which is triggered by changes in hydrophobic and hydrogen bond interactions. Since the hydrophobic of Ce6 can decrease the thermal phase-transition temperature of PNIPAM, we only consider introducing lower doping concentration of Ce6 in the nanogel. Moreover, the AMPS as monomes was chosen to adjust the LUST and maintain the stability of nanogel-Ce6 during the blood circulation. Based on this, we used the volume phase-transition temperature (VPTT) to estimate the phase-transition properties due to VPTT is a key parameter of PNIPAM-based materials as drug carriers in clinical medicine. As depicted in Fig. 1b, the nanogel-Ce6 presents a 37.8 ℃, which is consistent with the value of Ce6 free nanogel [31], indicating that the introduction of 3 % Ce6 (feeding rate, w/w) in the nanogel system has no effect on VPTT. This ensures the blood circulation stability of nanogel-Ce6 under physiological conditions.

Importantly, the properties of PSs are the most basic prerequisite for PDT treatment. To demonstrate that Ce6 was successfully polymerized in nanogel, we performed the Ce6 release profile from nanogel-Ce6 and nanogel/Ce6 (encapsulation), respectively and the results are shown in Fig. 1c. After 24 h, 54.38 % of Ce6 is released from the nanogel/Ce6 against PBS buffer. However, a very slight Ce6 release was observed in the nanogel-Ce6 under the same condition. Furthermore, the polymerized Ce6 was further confirmed by the Fourier Transform infrared spectroscopy (FTIR) as shown in Fig. 1d. Since only a small amount of Ce6 (below 5 %) was involved in the polymerization, most of the characteristic peaks of Ce6 was not obvious. But we can still find that the vibration in 2974 cm^{-1} assigned to the CH_3 enhanced and the vibration of −COOH groups of Ce6 in 3430 cm^{-1}. The variance of the FTIR analysis results confirmed the formation of nanogel-Ce6.

The advantages of nanogel as a PDT carrier can be demonstrated by its spectral properties of Ce6 in different forms, as shown in Fig. 2. Ce6 in DMF is the monomeric state as indicated by a single, sharp Soret band at 410 nm and also at 660 nm. In PBS, Ce6 occurs as dimers/aggregates and shows a blue shift around 650 nm. Due to the amphiphilic nature of Ce6, it is easy to aggregate in aqueous solution under intermolecular force, in particular, the H-aggregation, resulting in the change of its excited state. Compared with the nanogel, a typical Ce6 absorption peak appears in nanogel-Ce6 with a monomer state, even at 5 % (w/w) concentrations (Fig. 3c). In comparison with free Ce6 in aqueous solution, no significant aggregation was observed in the 1 − 5 wt % range of Ce6 in nanogel-Ce6, as indicated by the sharp Soret band at 410 nm. Additionally, the fluorescence emission intensity of Ce6-based nanoparticles demonstrated the advance of nanogel-Ce6 as the

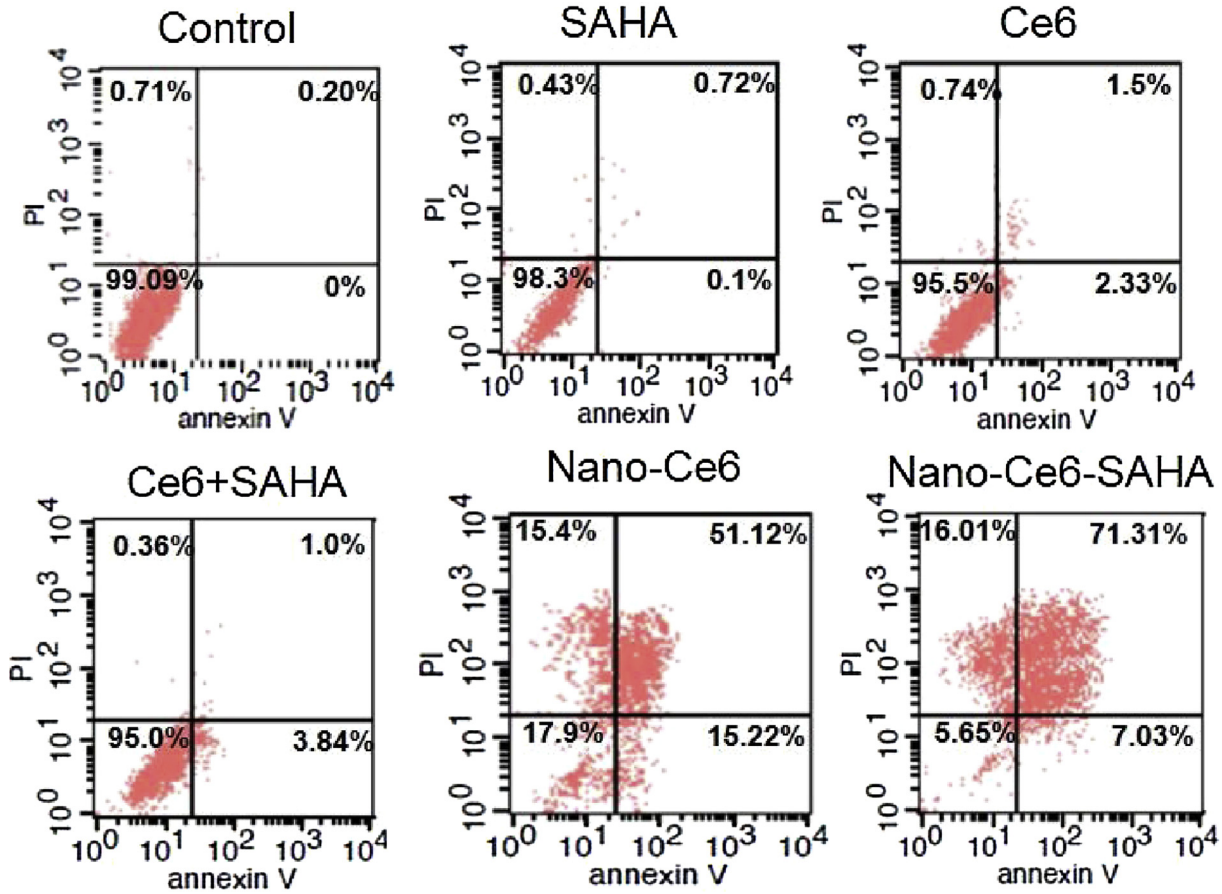

Fig. 6. Relative apoptosis of cells with different treatments after being incubated with saline; SAHA; Ce6 + 655nm laser; Ce6 + SAHA + 655nm laser; nanogel-Ce6 and nanogel-Ce6-SAHA + 655nm laser. Excitation power density = 50mW/cm^2. The PC-3 cells were stained by Annexin V-FITC and PI then analyzed by flow cytometer.

carrier. There are only 8.17 % in PBS and 45.1 % in nanogel-Ce6 of emission intensity in comparison with the Ce6 in DMF (set as 100 %).

3.2. Singlet oxygen detection

Next, we evaluated the generation of singlet oxygen through the DPBF consumption method [5]. DPBF consumption measured at 417 nm over time in solutions of nanogel-Ce6 with different amounts of Ce6, and free Ce6 in PBS. Upon 655 nm light irradiation, the relative singlet oxygen quantum yields (ΦΔ) of the nanogel-Ce6 nanoparticles were calculated from the slope of the DPBF consumption and the Ce6 in PBS as the control. Fig. 2c shows the decrease in DPBF absorption overtime for the above samples. Among of them, nanogel-Ce6 (3 %, w/w) presents the maximum slope, indicating the optimal doping concentration in nanogel networks for PDT, although it shows neither the strongest emission nor the highest loading efficiency (Fig. 2d) due to the aggregation-caused quenching (ACQ) effect of Ce6.

3.3. GSH triggered SAHA release from nanogel-Ce6-SAHA nanoplatform

BAC as the GSH sensitive cross-linker was incorporated into the nanogels for stimuli-responsive drug release. Nanogel-Ce6-SAHA nanoplatform dissolved in PBS (pH = 7.4) with variable GSH concentrations was measured, as shown in Fig. 3a. Compared with the free SAHA group, the cumulative release of SAHA without GSH (0 mM) was 41 % in 2 h and 91 % in 20 h, respectively. The results confirmed the obvious sustained release effect of nanoplatform. Moreover, after stimuli with 10 mM and 30 mM of GSH, SAHA release from nanoplatform reached 51 % and 62 % in 2 h, respectively, and the amount of accumulative release accelerated obviously due to the cleavage of the S—S bond in the cross-linked network of nanogel-Ce6 by reductive GSH and decline of interaction between SAHA and nanogel.

3.4. Cellular uptake

To demonstrate the advantage of the nanogel-Ce6, we observed the cellular uptake of Ce6 and nanogel-Ce6 with different time incubation, which was identified by the fluorescence intensity of Ce6 with the same test parameter. After 3 h and 6 h incubation, respectively, the cells were collected and imaged by a confocal fluorescence microscope. Compared with free Ce6 groups, rather strong red fluorescence signals appeared in the cytoplasm of cells at 3 h, suggesting the efficient cellular uptake of nanogel-Ce6 nanoparticles (Fig. 4). We can find that there is no significant fluorescence enhancement after another 3 h incubation, indicating the good uptake profile of nanogel-Ce6 within 3 h. While the free Ce6 group shows weaker fluorescence due to the aggregates of Ce6 in an aqueous medium. This result further demonstrates the advantages of nanogel-Ce6 for PDT.

3.5. Effects of SAHA combined with nanogel-Ce6-mediated PDT on prostate cancer cell viability in vitro

To determine the antitumor activity of nanogel-Ce6-SAHA, CCK8 assay was performed to analyze the cell viability. Dark toxicity was evaluated as shown in Fig. S2 (ESI). Nanogel-Ce6 or nanogel-Ce6-SAHA showed no significant changes in cell viability at a dose of 10 mg/mL. SAHA (5 μM) and Ce6 (3 μg/mL) treatment groups exhibited no significant anti-proliferative effect for 24 h treatment post-irradiation, and the same results were also observed in SAHA and Ce6 combination group. However, nanogel-Ce6 exhibited a significant inhibitory effect

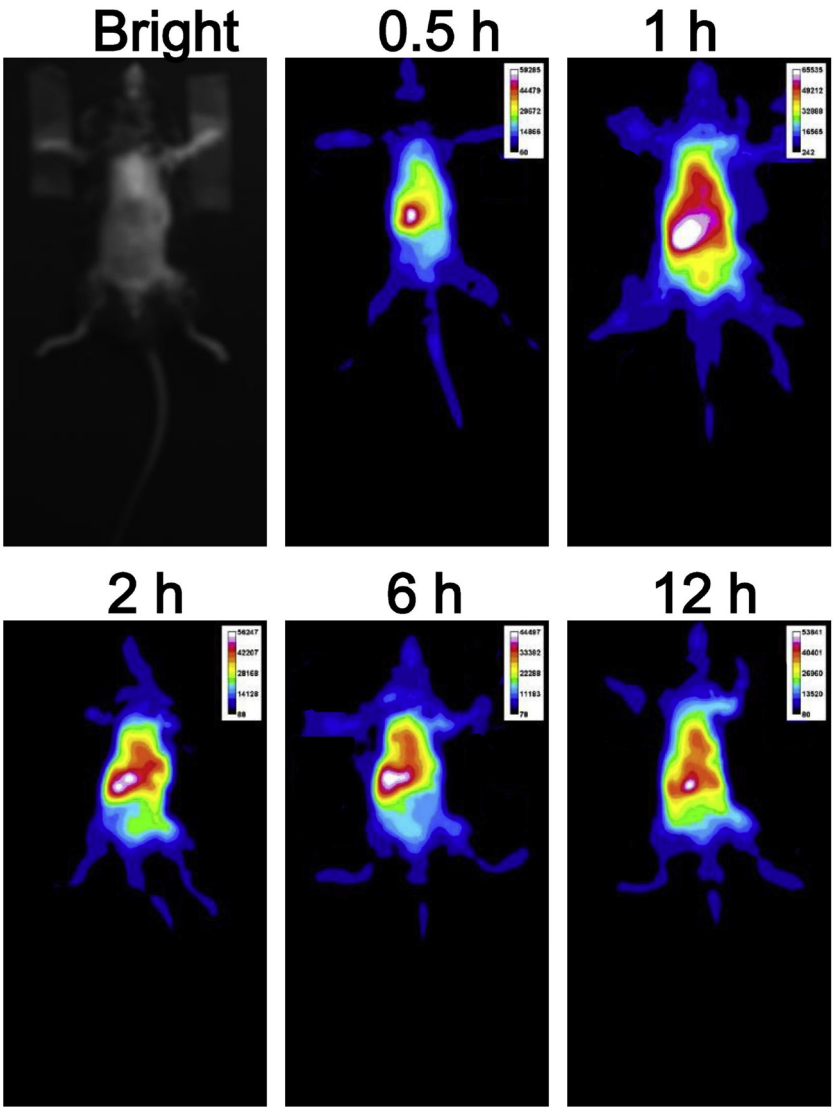

Fig. 7. Fluorescence images of normal C57/BL6 mice after the injection of nanoplatforms from the bright field, 0.5h, 1h, 2h, 6h, and 12h, which was obtained using a CMOS camera coupled with a 700nm long-pass filter under 655nm excitation.(Non-color images were provided in supplementary information as Figure S3).

on cell growth, and the effect was enhanced when the time of irradiation was increased from 10 s to 20 s, which reduced cell viability up to 72 % and 30 %, respectively (Fig. 5). Notably, nanogel-Ce6-SAHA exhibited greater antitumor effect compared with the nanogel-Ce6 only group, the cell viability was reduced to 40 % and 8 % after irradiation for 10 s or 20 s (Fig. 5). These results demonstrated a strong synergistic interaction between SAHA and PDT with 10 mg/mL nanogel-Ce6.

3.6. Nanogel-Ce6-SAHA enhanced tumor cells apoptosis

Followed by PDT, the tumor cells activate cell death pathways, such as apoptosis, necrosis, and autophagy-associated cell death. Apoptosis has been shown to be an important route of cellular death in response to PDT. Since nanogel-Ce6 combined SAHA with irradiation exhibited stronger synergism in cell viability, the apoptosis of tumor cells was further studied. PC-3 cells were incubated respectively with Ce6, SAHA, nanogel-Ce6, nanogel-Ce6-SAHA for 4 h, followed by 655 nm laser irradiation at 50 mW/cm2 for 15 s. Quantification of apoptotic cells based on Annexin V and PI staining is shown in Fig. 6. It can be found that no apoptotic cells were detected in the SAHA alone group, only 3.38 % of apoptotic cells in Ce6 and 4.84 % of Ce6 + SAHA group were detected after PDT treatment, whereas nanogel-Ce6 group showed a higher level of apoptotic cells (66.34 %). 78.34 % of apoptotic cells were observed in nanogel-Ce6-SAHA group, which was much higher than that of nanogel-Ce6 alone group. These results suggested that nanogel-Ce6 dramatically improved PDT efficacy in comparison with free Ce6. Notably, SAHA and nanogel-Ce6 exhibited synergism against the tumor cells which resulted in a strong pro-apoptotic effect induced by PDT.

3.7. Imaging and antitumor efficacy in vivo

Prior to evaluating the HDACi synergistic photodynamic therapy of PCa by nanogel-Ce6-SAHA, we performed the optical imaging in normal and RM-1 tumor-bearing C57/BL6 mice. The normal mice were *i.v.* injected with nanogel-Ce6-SAHA and the fluorescence imaging was recorded, as shown in Fig. 7 (Non-color images, as shown in Fig. S3 in supplementary information). The fluorescence from the nanoparticle was mainly distributed in the spleen and the liver after post-injection. This phenomenon was also observed in previous studies using other nanoparticles [32]. Nanoparticle uptake is mainly operated by liver Kupffer cells, but splenic macrophages also have a similar function [33]. The maximum fluorescence was observed in the first 1–2 h, and then the fluorescence gradually decreased *in vivo* (6 − 12 h), indicating

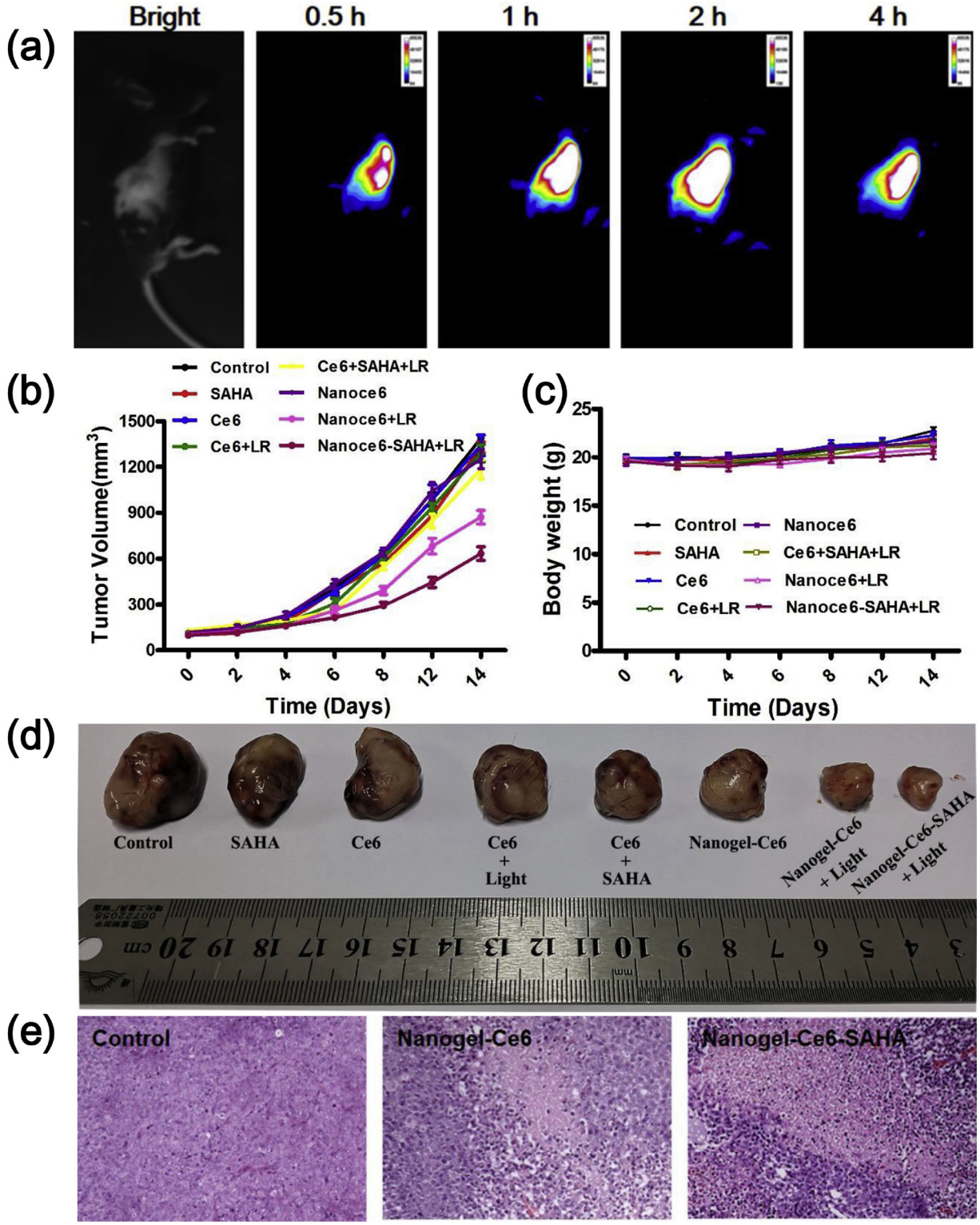

Fig. 8. (a) Images of RM-1 tumor-bearing micelle after 4 h post-injection (b) Tumor growth curves in different treatment groups, (n = 5). (c) Bodyweight curves of mice with RM-1 tumors in each group. (d)Tumors from representative mice after various treatments. (e) H&E staining of tumor sections from different treatment groups.

the metabolism of nanoplatforms.

Afterward, we further evaluated the accumulation of nanoplatforms in the tumor site after post-injection. Fig. 8a showed the *in vivo* tumor-targeted fluorescence imaging effects after post-injection, indicating the potential application of imaging-guided PDT therapy by exploring nanogel-Ce6-SAHA nanoplatform. After that, for PDT groups, the mice were *i.v.* injected with Ce6, SAHA, nanogel-Ce6, and nanogel-Ce6-SAHA respectively. The groups injected with Ce6 or nano-Ce6 without irradiation and no treatment group was all set as controls. Under the guidance of fluorescence imaging, the light can be precisely focused on the tumor region and the starting time of PDT can be set after 2 h post-injection of nanogel-Ce6-SAHA. On the base of these, the mice were

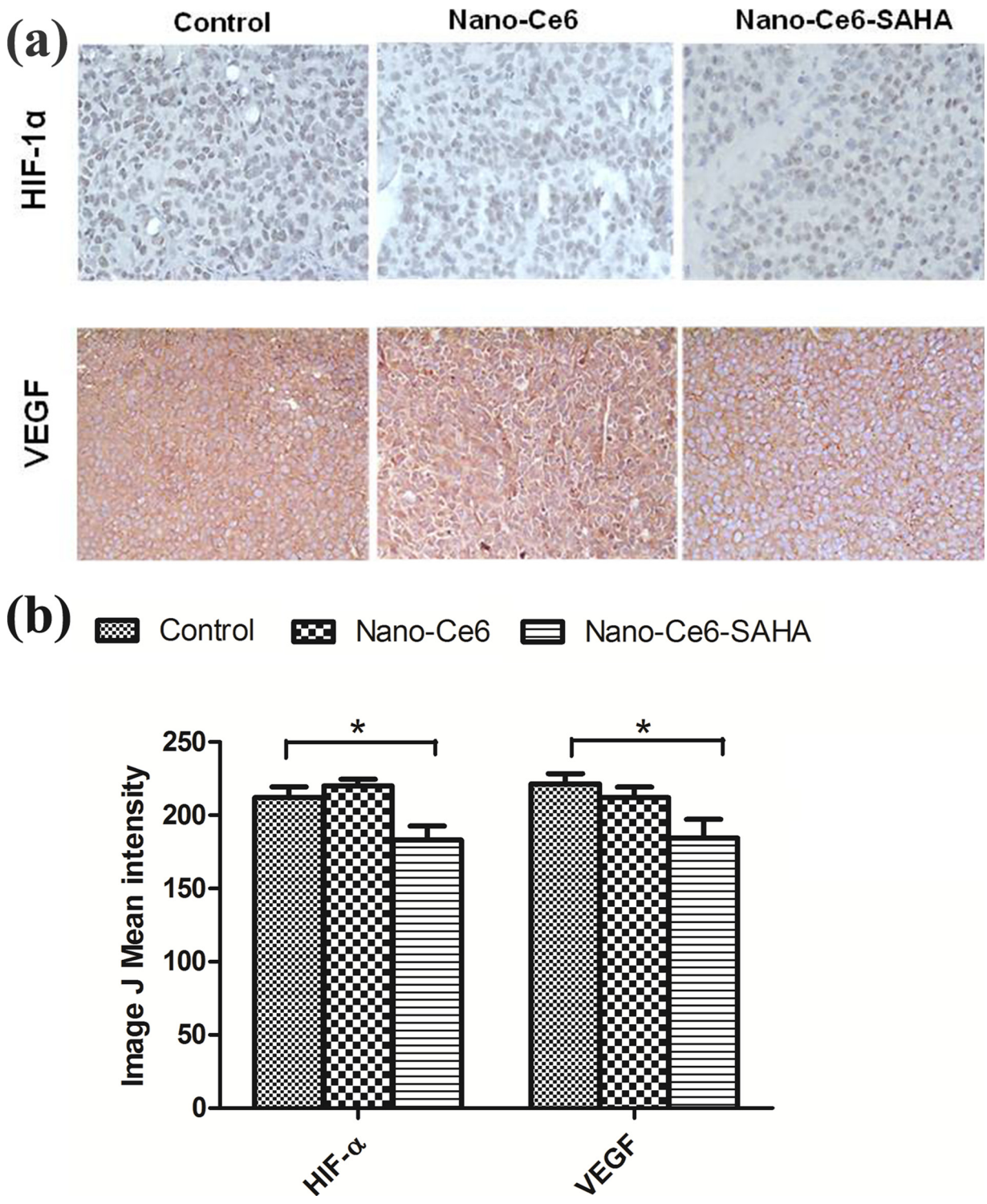

Fig. 9. IHC analysis of HIF-1α and VEGF expression in tumors. (a) Representative immunohistochemical staining for HIF-1α and VEGF in tumor tissues with different treatments (×200). (b) The quantification of IHC images was performed using Image *J* software. Columns indicate quantitative analysis in different tumors per group n = 5; *P < 0.05.

illuminated with an irradiance of 50 mW/cm^2 light at 655 nm for 240 s at 12 h post-injection. The tumor volumes in control groups increased remarkably during the process. As can be seen in Fig. 8b, SAHA treatment group showed no obvious effect on the growth of tumors compared with control mice, it may be related to a single injection of SAHA, which could not produce a constant effect. As shown in Fig. 8c, we did not notice any obvious changes in body weight in the nano-ce6-SAHA with irradiation group, which indicated the biosafety of the combined treatment strategy.

For Ce6 and Ce6 + SAHA with irradiation groups, the tumors were only minor suppressed, which demonstrated that the Ce6 was insufficient to inhibit tumor growth because of quick body clearance or less tumor-selective property. The tumor volume in the nanogel-Ce6 group grew more slowly and the group received the injection of nanogel-Ce6-SAHA grew most slowly compare with the other groups. On the 14th day after treatment, the size of excised tumors with nanogel-

Ce6-SAHA mediated PDT treatment was much smaller than the other groups (Fig. 8d). Excised tumors were weighed, the results indicated significantly lower tumor weight in mice injected with nanogel-Ce6-SAHA compared with other groups ($P < 0.05$) (Fig. S4). These results suggested SAHA enhanced the susceptibility of nanogel-Ce6 which significantly inhibited tumor growth.

Histological analysis of the tumors showed a mass of cellular necrosis in nanogel-Ce6-SAHA group, which is different from the control group and nanogel-Ce6 group (Fig. 8e). Inflammatory cell infiltration was also observed in the area of necrosis. There were no obvious pathological changes of the livers, kidneys, and spleens (data not shown), which illustrated that the nanogel-Ce6-SAHA was relatively safe for mice.

3.8. Immunohistochemical analysis

Tumor growth and metastasis depend on angiogenesis [34]. Angiogenesis is triggered by hypoxia or hypoxic microenvironment, and the cellular response to hypoxia is primarily regulated by HIF-1α [35,36]. The HIF-1α pathway was activated though PDT-induced tissue hypoxia [27]. HDACis have been showed to inhibit the nuclear translocation of HIF-1α, in the meantime, negatively regulate the mRNA levels HIF-1α, which will further decrease the transcription of VEGF mRNA. To further investigate the effect of nanogel-Ce6-SAHA mediated PDT on HIF-1α and VEGF protein expression in vivo, immunohistochemical staining was analyzed on tissue slices of tumors excised from three groups. Based on the results of in vivo anti-tumor experiment, we only observed the pathology and histology of tumor tissues of nanogel-Ce6 and nanogel-ce6-SAHA group. As showed in Fig. 9, HIF-1α is localized mainly in the nucleus of tumor cells, but VEGF is expressed in the cytoplasm and cell membrane. In the control group, strongly positive staining for HIF-1α and VEGF were detected. There was no significant difference between nanogel-Ce6 and the control group. However, nanogel-Ce6-SAHA mediated PDT dramatically inhibited the expression of HIF-1α and VEGF compared with the other groups. These results suggested that nanogel-Ce6-SAHA mediated PDT can inhibit the survival signaling which was induced by HIF pathway after PDT treatment. In the meantime, the expression of HIF-1α target gene VEGF was also decreased which induced the anti-angiogenic effect on tumor progression.

4. Conclusions

In summary, we have demonstrated that the photosensitizer—Ce6 was polymerized in the nanogel network as the nanophotosensitizers and drug carrier for PDT and drug payloads. The as-obtained nanogel-Ce6 nanoplatform offers highly effective singlet oxygen yield towards PDT treatment of cancer when compared to free Ce6. The introduction of SAHA, an HADC inhibitor as drug payload to improve the antitumor efficacy via inhibiting HIF-1α and VEGF pathways of tumor cells involved in PDT resistance. This study offers a synergistic tumor treatment strategy and paves the way towards addressing the main hindrance to the practical application of PDT and small molecular drug delivery.

Contributions

Nian Liu performed experiments, analyzed data, and wrote the manuscript. Hongsen Liu performed mouse injections and imaging. Haoran Chen performed spectroscopic experiment. Gang Wang and Haolin Teng performed H&E and IHC analysis. Yulei Chang designed experiments and wrote the manuscript.

Declaration of Competing Interest

The authors declare that there are no conflicts of interest.

Acknowledgements

This work was supported by the National Natural Science Foundation of China (grants 11674316, 61875191, 51772122, 11874354, 11874355, 61575194 and 11604331) and Project of Science and Technology Agency, Jilin Province (20180101222JC)

Appendix A. Supplementary data

Supplementary material related to this article can be found, in the online version, at doi:https://doi.org/10.1016/j.colsurfb.2019.110753.

References

[1] Z. Zhou, J. Song, L. Nie, X. Chen, Reactive oxygen species generating systems meeting challenges of photodynamic cancer therapy, Chem. Soc. Rev. 45 (23) (2016) 6597–6626.
[2] A.G. Denkova, R.M. de Kruijff, P. Serra-Crespo, Nanocarrier-mediated photochemotherapy and photoradiotherapy, Adv. Healthc. Mater. 7 (8) (2018) e1701211.
[3] S. Monro, K.L. Colon, H. Yin, J. Roque 3rd, P. Konda, S. Gujar, R.P. Thummel, L. Lilge, C.G. Cameron, S.A. McFarland, Transition metal complexes and photodynamic therapy from a tumor-centered approach: challenges, opportunities, and highlights from the development of TLD1433, Chem. Rev. 119 (2) (2019) 797–828.
[4] X. Li, S. Lee, J. Yoon, Supramolecular photosensitizers rejuvenate photodynamic therapy, Chem. Soc. Rev. 47 (4) (2018) 1174–1188.
[5] X. Liu, Z. Fan, L. Zhang, Z. Jin, D. Yan, Y. Zhang, X. Li, L. Tu, B. Xue, Y. Chang, H. Zhang, X. Kong, Bcl-2 inhibitor uploaded upconversion nanophotosensitizers to overcome the photodynamic therapy resistance of cancer through adjuvant intervention strategy, Biomaterials 144 (2017) 73–83.
[6] K. Plaetzer, B. Krammer, J. Berlanda, F. Berr, T. Kiesslich, Photophysics and photochemistry of photodynamic therapy: fundamental aspects, Lasers Med. Sci. 24 (2) (2009) 259–268.
[7] J. Zuo, L. Tu, Q. Li, Y. Feng, I. Que, Y. Zhang, X. Liu, B. Xue, L.J. Cruz, Y. Chang, H. Zhang, X. Kong, Near infrared light sensitive ultraviolet-blue nanophotoswitch for imaging-guided “Off-On” therapy, ACS Nano 12 (4) (2018) 3217–3225.
[8] L. Milla Sanabria, M.E. Rodriguez, I.S. Cogno, N.B. Rumie Vittar, M.F. Pansa, M.J. Lamberti, V.A. Rivarola, Direct and indirect photodynamic therapy effects on the cellular and molecular components of the tumor microenvironment, Biochim. Biophys. Acta 1835 (1) (2013) 36–45.
[9] R.D. Almeida, B.J. Manadas, A.P. Carvalho, C.B. Duarte, Intracellular signaling mechanisms in photodynamic therapy, Biochim. Biophys. Acta 1704 (2) (2004) 59–86.
[10] M.J. Garland, C.M. Cassidy, D. Woolfson, R.F. Donnelly, Designing photosensitizers for photodynamic therapy: strategies, challenges and promising developments, Future Med. Chem. 1 (4) (2009) 667–691.
[11] T. Gheewala, T. Skwor, G. Munirathinam, Photosensitizers in prostate cancer therapy, Oncotarget 8 (18) (2017) 30524–30538.
[12] L. Lamch, A. Pucek, J. Kulbacka, M. Chudy, E. Jastrzebska, K. Tokarska, M. Bulka, Z. Brzozka, K.A. Wilk, Recent progress in the engineering of multifunctional colloidal nanoparticles for enhanced photodynamic therapy and bioimaging, Adv. Colloid Interface Sci. 261 (2018) 62–81.
[13] F. Schmitt, L. Lagopoulos, P. Kauper, N. Rossi, N. Busso, J. Barge, G. Wagnieres, C. Laue, C. Wandrey, L. Juillerat-Jeanneret, Chitosan-based nanogels for selective delivery of photosensitizers to macrophages and improved retention in and therapy of articular joints, J. Control. Release 144 (2) (2010) 242–250.
[14] J.D. Spikes, New trends in photobiology, J. Photochem. Photobiol. B Biol. 6 (3) (1990) 259–274.
[15] K. Yang, T. Niu, M. Luo, L. Tang, L. Kang, Enhanced cytotoxicity and apoptosis through inhibiting autophagy in metastatic potential colon cancer SW620 cells treated with Chlorin e6 photodynamic therapy, Photodiagn. Photodyn. Ther. 24 (2018) 332–341.
[16] M. Molina, M. Asadian-Birjand, J. Balach, J. Bergueiro, E. Miceli, M. Calderón, Stimuli-responsive nanogel composites and their application in nanomedicine, Chem. Soc. Rev. 44 (17) (2015) 6161–6186.
[17] L. Zhou, H. Wang, Y. Li, Stimuli-responsive nanomedicines for overcoming cancer multidrug resistance, Theranostics 8 (4) (2018) 1059–1074.
[18] W. Hou, F. Xia, C.S. Alves, X. Qian, Y. Yang, D. Cui, MMP2-targeting and redox-responsive PEGylated chlorin e6 nanoparticles for cancer near-infrared imaging and photodynamic therapy, ACS Appl. Mater. Interfaces 8 (2) (2016) 1447–1457.
[19] C. Feng, D. Zhu, L. Chen, Y. Lu, J. Liu, N.Y. Kim, S. Liang, X. Zhang, Y. Lin, Y. Ma, C. Dong, Targeted delivery of chlorin e6 via redox sensitive diselenide-containing micelles for improved photodynamic therapy in cluster of differentiation 44-over-expressing breast cancer, Front. Pharmacol. 10 (2019) 369.
[20] H. Yang, Q. Wang, S. Huang, A. Xiao, F. Li, L. Gan, X. Yang, Smart pH/Redox dual-responsive nanogels for on-demand intracellular anticancer drug release, ACS Appl. Mater. Interfaces 8 (12) (2016) 7729–7738.
[21] Y. Zhao, C. Zheng, Q. Wang, J. Fang, G. Zhou, H. Zhao, Y. Yang, H. Xu, G. Feng, X. Yang, Permanent and peripheral embolization: temperature-sensitive p(N-Isopropylacrylamide-co-butyl Methylacrylate) nanogel as a novel blood-vessel-embolic material in the interventional therapy of liver tumors, Adv. Funct. Mater. 21

(11) (2011) 2035–2042.
[22] J. Peng, T. Qi, J. Liao, B. Chu, Q. Yang, W. Li, Y. Qu, F. Luo, Z. Qian, Controlled release of cisplatin from pH-thermal dual responsive nanogels, Biomaterials 34 (34) (2013) 8726–8740.
[23] R. Xing, K. Liu, T. Jiao, N. Zhang, K. Ma, R. Zhang, Q. Zou, G. Ma, X. Yan, An injectable self-assembling collagen-gold hybrid hydrogel for combinatorial antitumor photothermal/photodynamic therapy, Adv. Mater. 28 (19) (2016) 3669–3676.
[24] S. Belali, A.R. Karimi, M. Hadizadeh, Novel nanostructured smart, photodynamic hydrogels based on poly(N -isopropylacrylamide) bearing porphyrin units in their crosslink chains: a potential sensitizer system in cancer therapy, Polymer 109 (2017) 93–105.
[25] A. Casas, G. Di Venosa, T. Hasan, B. Al, Mechanisms of resistance to photodynamic therapy, Curr. Med. Chem. 18 (16) (2011) 2486–2515.
[26] M.J. Lamberti, M.F. Pansa, R.E. Vera, M.E. Fernandez-Zapico, N.B. Rumie Vittar, V.A. Rivarola, Transcriptional activation of HIF-1 by a ROS-ERK axis underlies the resistance to photodynamic therapy, PLoS One 12 (5) (2017) e0177801.
[27] A. Ferrario, K.F. von Tiehl, N. Rucker, M.A. Schwarz, P.S. Gill, C.J. Gomer, Antiangiogenic treatment enhances photodynamic therapy responsiveness in a mouse mammary carcinoma, Cancer Res. 60 (15) (2000) 4066–4069.
[28] P. Agostinis, K. Berg, K.A. Cengel, T.H. Foster, A.W. Girotti, S.O. Gollnick, S.M. Hahn, M.R. Hamblin, A. Juzeniene, D. Kessel, M. Korbelik, J. Moan, P. Mroz, D. Nowis, J. Piette, B.C. Wilson, J. Golab, Photodynamic therapy of cancer: an update, CA Cancer J. Clin. 61 (4) (2011) 250–281.
[29] C. Zhang, C. Yang, M.J. Feldman, H. Wang, Y. Pang, D.M. Maggio, D. Zhu, C.L. Nesvick, P. Dmitriev, P. Bullova, P. Chittiboina, R.O. Brady, K. Pacak, Z. Zhuang, Vorinostat suppresses hypoxia signaling by modulating nuclear translocation of hypoxia inducible factor 1 alpha, Oncotarget 8 (34) (2017) 56110–56125.
[30] D.M. Hutt, D.M. Roth, H. Vignaud, C. Cullin, M. Bouchecareilh, The histone deacetylase inhibitor, Vorinostat, represses hypoxia inducible factor 1 alpha expression through translational inhibition, PLoS One 9 (8) (2014) e106224.
[31] C. Zhang, Q. Li, Y. Zhao, H. Liu, S. Song, Y. Zhao, Q. Lin, Y. Chang, Near-infrared light-mediated and nitric oxide-supplied nanospheres for enhanced synergistic thermo-chemotherapy, J. Mater. Chem. B 7 (4) (2019) 548–555.
[32] L.F. Shen, Y.D. Zhang, H.J. Shen, S. Zeng, X. Wang, C. Wang, Y. Le, H. Shen, Liver targeting and the delayed drug release of the nanoparticles of adriamycin polybutylcyanoacrylate in mice, Chin. Med. J. (Engl.) 119 (15) (2006) 1287–1293.
[33] M. Cataldi, C. Vigliotti, T. Mosca, M. Cammarota, D. Capone, Emerging role of the spleen in the pharmacokinetics of monoclonal antibodies, nanoparticles and exosomes, Int. J. Mol. Sci. 18 (6) (2017) 1249.
[34] J.B. Aragon-Ching, R.A. Madan, W.L. Dahut, Angiogenesis inhibition in prostate cancer: current uses and future promises, J. Oncol. 2010 (2010) 361836.
[35] L. Schito, G.L. Semenza, Hypoxia-inducible factors: master regulators of cancer progression, Trends Cancer 2 (12) (2016) 758–770.
[36] L. Liu, Z. Liang, K. Guo, H. Wang, Relationship between the expression of CD133, HIF-1alpha, VEGF and the proliferation and apoptosis in hypoxic human prostate cancer cells, Oncol. Lett. 14 (4) (2017) 4065–4068.